

Effect of magnetic field on expansion of ferrofluid-encapsulated microbubble

Zhiwei Du(杜芷玮), Fan Li(李凡), Ruiqi Pan(潘瑞琪), Runyang Mo(莫润阳), and Chenghui Wang(王成会)
Citation: Chin. Phys. B, 2023, 32 (**6**): 064302. DOI: 10.1088/1674-1056/acc1d2
Journal homepage: http://cpb.iphy.ac.cn; http://iopscience.iop.org/cpb

What follows is a list of articles you may be interested in

Wideband frequency-dependent dielectric properties of rat tissues exposed to low-intensity focused ultrasound in the microwave frequency range

Xue Wang(王雪), Shi-Xie Jiang, Lin Huang(黄林), Zi-Hui Chi(迟子惠), Dan Wu(吴丹), and Hua-Bei Jiang
Chin. Phys. B, 2023, 32 (**3**): 034305. DOI: 10.1088/1674-1056/ac7453

Quantitative ultrasound brain imaging with multiscale deconvolutional waveform inversion

Yu-Bing Li(李玉冰), Jian Wang(王建), Chang Su(苏畅), Wei-Jun Lin(林伟军), Xiu-Ming Wang(王秀明), and Yi Luo(骆毅)
Chin. Phys. B, 2023, 32 (**1**): 014303. DOI: 10.1088/1674-1056/ac6dad

Effects of adjacent bubble on spatiotemporal evolutions of mechanical stresses surrounding bubbles oscillating in tissues

Qing-Qin Zou(邹青钦), Shuang Lei(雷双), Zhang-Yong Li(李章勇), and Dui Qin(秦对)
Chin. Phys. B, 2023, 32 (**1**): 014302. DOI: 10.1088/1674-1056/ac70ba

High-efficiency unidirectional wavefront manipulation for broadband airborne sound with a planar device

Yang Tan(谭杨), Bin Liang(梁彬), and Jianchun Cheng(程建春)
Chin. Phys. B, 2022, 31 (**3**): 034303. DOI: 10.1088/1674-1056/ac1e14

Nonlinear oscillation characteristics of magnetic microbubbles under acoustic and magnetic fields

Lixia Zhao(赵丽霞), Huimin Shi(史慧敏), Isaac Bello, Jing Hu(胡静), Chenghui Wang(王成会), and Runyang Mo(莫润阳)
Chin. Phys. B, 2022, 31 (**3**): 034302. DOI: 10.1088/1674-1056/ac1f01

Effect of magnetic field on expansion of ferrofluid-encapsulated microbubble

Zhiwei Du(杜芷玮), Fan Li(李凡), Ruiqi Pan(潘瑞琪), Runyang Mo(莫润阳)[†], and Chenghui Wang(王成会)

Shaanxi Key Laboratory of Ultrasonics, Shaanxi Normal University, Xi'an 710119, *China*

(Received 16 November 2022; revised manuscript received 19 February 2023; accepted manuscript online 7 March 2023)

Magnetic microbubbles (MMBs) have great potential applications in drug delivery and target therapy because they can be controlled by magnetic fields. In this paper, dynamic equations are derived by Lagrangian formalism and the behavior of MMBs subject to a combination field of magnetic and ultrasound field in an incompressible infinite fluid is analyzed numerically. The results show that the magnetic field can promote bubble expansion and hinder its translational motion, and both the enhancement and obstruction effects will weaken with the decrease of bubble size. The initial translational velocity has almost no effect on bubbles motion. Besides, the maximum expansion radius of MMBs increases with the ferrofluid shell thickness, while that of the common MBs is just the opposite. In addition, the periodic change of Levich viscous drag caused by the rebound leads to the step-like translational motion. Finally, the ferrofluid-shell model can be replaced by the model of non-magnetic microbubbles in magnetic liquid at high driving frequency.

Keywords: magnetic microbubbles, ultrasound, magnetic field, translational motion

PACS: 43.25.+y, 43.35.+d, 47.55.dd **DOI:** 10.1088/1674-1056/acc1d2

1. Introduction

Microbubbles (MBs) were initially developed as contrast agents (UCAs) to enhance imaging of the vasculature. Recently, MBs have been functionalised by attachment of antibodies, drugs or other nanoparticles and used as drug delivery platform or sonodynamic therapy.[1,2] Magnetic MBs consist of gas cavities 1 μm–10 μm in diameter stabilized by a surfactant, lipid and/or polymer coating, and magnetic iron oxide nanoparticles (IONPs) were incorporated into MBs. In fact, numerous formulations have been proposed to facilitate the loading of IONPs within the MB coating and/or on its surface and lead to different structures. Three main types of MMBs are:[3] IONPs in the oil phase under the shell (OilMBs), embedded in the phospholipid layer (LipMBs), and bound to the outer surface (SurfMBs). Experimental results show that the Surf-MBs have the strongest response to external magnetic field, followed by OilMBs but with improved stability.[3,4] Vlaskou[5] believes that LipMBs have stronger ultrasonic contrast than other structures.

MMBs can be guided or controlled by an external magnetic field, it also undergoes volumetric oscillations when exposed to a US field. For its versatility, MMBs have been applied or experimentally studied in various diagnostic, therapeutic, and genetic aspects, such as anticancer drug delivery,[6–8] dual-mode angiography,[9–11] and thrombolysis,[12–15] which have achieved good results. However, there are few studies on its mechanism, which is related to the vibration and movement in blood vessel. Yang[16] confirmed that the steady cavitation threshold and inertial cavitation threshold of MMBs decreased with the increase of IONPs concentration and drive acoustic pulse length. In whole blood, Owen[17] found that the number of retained MMBs would decrease under a given combination of vessel diameter, flow rate and shear rate. A higher magnetic field and magnetic field gradient or a greater quantity of bubbles were needed to compensate for this effect. Stride *et al.*[18] experimentally studied the effects of ultrasound and magnetic field on gene delivery and they showed that the combination of IONPs could accelerate the transfection.

With respect to the great potential as a minimally invasive drug, it is urgent to deeply understand its dynamic mechanism, not only more applied experimental studies but also better theoretical models are needed. In the early stages, the shell was assumed to be a continuous incompressible elastic solid material. Church[19] gave an oscillation equation of the encapsulated microbubble. Doinikov[20] developed coupling equations to describe the coupled motion of vibration and translational motion by Lagrange equation. He also proposed a model describing bubble encapsulation using linear Maxwell constitutive equations.[21] For the MBs with IONPs, one way to study the dynamic is to treat it as a non-magnetic bubble in ferrofluid.[22,23] This alternative provides a convenient experimental scheme for MMBs, and Steven[22] tried to derive the generalized Bernoulli equation including the effects of surface tension and the applied magnetic field to investigate the dynamics of non-spherical MBs in ferrofluid. However, it remains to be seen whether this indirect method can demonstrate the response of MMBs realistically. Zhao[24] attempted to build a direct theoretical model for a MMBs based on the multilayer membranes structural properties and studied its oscillation in magnetic field and ultrasound field. Mulvana *et al.*[25] conducted a preliminary vibration model of MMBs by considering the influence of nanoparticles on membrane den-

[†]Corresponding author. E-mail: mmrryycn@snnu.edu.cn

© 2023 Chinese Physical Society and IOP Publishing Ltd

sity. Unfortunately, translational motion and coupling effects with oscillation were not considered in these works.

As a continuation and development, in this study, OilMBs mentioned in the literature[3] is take as an example of MMBs, the dynamic equations of translation and oscillation in magnetic and ultrasound field are deduced by Lagrange method, the influence of magnetic field on MMBs' motion is investigated.

2. Theoretical model

When the bubble diameter is very small, the non-sphericity becomes negligible because the surface tension on the bubble is greater than the other forces. Suppose a multi-layer spherical MMBs with inner radius R_{10} and outer radius R_{20} in an infinite and incompressible liquid (see Fig. 1). The inner part 1 is filled with air, layer 2 is ferrofluid and the viscosity and permeability are η_s and μ, respectively. The density of superparamagnetic iron oxide (SPIOs) nanoparticles is ρ_s. Layer 3 is a hydrophobic phospholipid layer with viscosity η_{s0}, and its thickness is negligible compared with layer 2. The thickness of the non-dimensional shell is $n = R_{20}/R_{10}$. In addition, the bubble is assumed to be translated with velocity v_x along x axis in the positive direction and spherical coordinates (r, θ, ϕ) with the origin at the center of the bubble are used to describe the motion of MMBs. A single MMBs is subjected to a combined field including a sine wave sound field $P_d = P_a \sin(2\pi ft)$ and an applied magnetic field $\boldsymbol{H}$. The strength of the applied magnetic field should be H_0 at infinity.

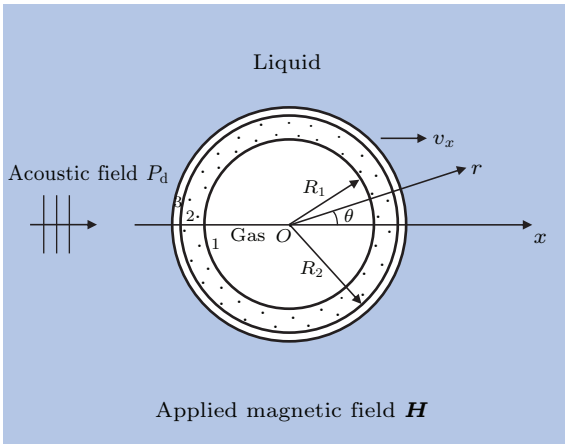


Fig. 1. Schematic diagram of a single MMB.

The bubble and its surrounding liquid form a system whose kinetic energy T is the sum of liquid kinetic energy T_L and bubble kinetic energy T_S. Considering that the air mass inside the bubble is much smaller than that of the shell, the kinetic energy of the bubble can be replaced by the kinetic energy of the shell:[20]

$$\begin{aligned} T &= T_L + T_S = 2\pi\rho_L R_2^3 \left(\dot{R}_2^2 + \frac{1}{6}\dot{x}^2\right) \\ &\quad + 2\pi\rho_s R_1^3 \dot{R}_1^2 \left(1 - \frac{R_1}{R_2}\right), \end{aligned} \tag{1}$$

where x is the position coordinate of bubble center in an inertial frame, and $\dot{x}$ is the translation velocity (or denoted as v_x). Total potential energy U of the system can be written as

$$U = -P_{sc} V_b - x F_{ex} + U_m, \tag{2}$$

where U_m is the magnetic potential energy, V_b is the bubble volume, F_{ex} is the external force acting on the bubble, and P_{sc} is the scattered pressure on the bubble surface. The pressure P_{sc} can be taken in the following form:[24,25]

$$\begin{aligned} P_{sc} &= \left(P_0 + \frac{2\sigma_1}{R_{10}} + \frac{2\sigma_2}{R_{20}}\right)\left(\frac{R_{10}}{R_1}\right)^{3\gamma} \\ &\quad - \frac{2\sigma_1}{R_1} - \frac{2\sigma_2}{R_2} - 4\eta_L \frac{\dot{R}_1 R_1^2}{R_2^3} \\ &\quad - 4\eta_s \frac{\dot{R}_1 \left(R_{20}^3 - R_{10}^3\right)}{R_2^3 R_1} - 4\eta_{s0} \frac{\dot{R}_2}{R_2^2} \\ &\quad - \frac{2K}{R_2}\left[1 - \left(\frac{R_{20}}{R_2}\right)^2\right] - P_0 - P_d, \end{aligned} \tag{3}$$

where P is static pressure, σ_1 and σ_2 are tension coefficients of the inner and outer surfaces respectively, γ is the polytropic exponent of the gas within the bubble, K is a constant related to the phospholipid layer, and η_L is viscosity of the liquid outside the bubble.

For a single bubble, the interaction between bubbles is ignored, F_{ex} is mainly Levich viscous drag and it was defined as[23]

$$F_{ex} = -12\pi\eta R_2(\dot{x} - v_{ex}), \tag{4}$$

with v_{ex} denoting the liquid velocity in x direction.

The magnetic potential energy U_m is expressed as $U_m = \int_{V_{all}} \frac{1}{2}\boldsymbol{H}\cdot\boldsymbol{B}\,\mathrm{d}V$. The magnetic field satisfies the following formulas: $\nabla^2\phi = 0$, $\boldsymbol{H} = -\nabla\phi$. Solving the Laplace equation of the magnetic scalar potential, the $\boldsymbol{H}$ in each region can be obtained as[24]

$$\boldsymbol{H} = \begin{cases} -a(\cos\theta\boldsymbol{e}_r - \sin\theta\boldsymbol{e}_\theta), & (r \le R_1), \\ \left(\dfrac{2c}{r^3} - b\right)\cos\theta\boldsymbol{e}_r + \left(b + \dfrac{c}{r^3}\right)\sin\theta\boldsymbol{e}_\theta, & (R_1 < r < R_2), \\ -\left(-H_0 - \dfrac{2d}{r^3}\right)\cos\theta\boldsymbol{e}_r + \left(-H_0 + \dfrac{d}{r^3}\right)\sin\theta\boldsymbol{e}_\theta, & (r \ge R_2). \end{cases} \tag{5}$$

It is assumed that $\boldsymbol{H}$ is continuous through the bubble interface, the coefficients a, b, c, and d can be given by

$$\begin{aligned}
a &= -\frac{9\mu\mu_0 H_0 R_2^3}{(2\mu+\mu_0)(2\mu_0+\mu)R_2^3 - 2(\mu-\mu_0)R_1^3},\\
b &= -\frac{3\mu_0(\mu_0+2\mu)H_0 R_2^3}{(2\mu+\mu_0)(2\mu_0+\mu)R_2^3 - 2(\mu-\mu_0)R_1^3},\\
c &= -\frac{3\mu_0(\mu-\mu_0)H_0 R_1^3 R_2^3}{(2\mu+\mu_0)(2\mu_0+\mu)R_2^3 - 2(\mu-\mu_0)R_1^3},\\
d &= \frac{(2\mu+\mu_0)(\mu-\mu_0)\left(R_2^3-R_1^3\right)H_0 R_2^3}{(2\mu+\mu_0)(2\mu_0+\mu)R_2^3 - 2(\mu-\mu_0)R_1^3}.
\end{aligned} \tag{6}$$

where μ is the vacuum permeability.

If the ferrofluid in layer 2 is isotropic, the magnetization $\boldsymbol{M}$ of a ferrofluid is a function of $\boldsymbol{H}$ in Langevin formula. The magnetic induction intensity $\boldsymbol{B}$ can be written as $B = \mu_0(H+M) = \mu_0(1+\chi)H$, here χ is the magnetic susceptibility of ferrofluid and taken to $\chi = \frac{M_s}{H}\left[\coth(\gamma_m H) - \frac{1}{\gamma_m H}\right]$, where M_s is saturation magnetization and γ_m is the initial value of magnetic susceptibility.[26] Then, the magnetic potential energy U_m can be expanded as

$$\begin{aligned}
U_m &= \frac{1}{2}\mu_0 a^2 V_1 + \frac{1}{2}(1+\chi)\mu_0\\
&\quad\times\left[(V_b - V_1)b^2 + \frac{8\pi}{3}c^2\left(\frac{1}{R_1^3} - \frac{1}{R_2^3}\right)\right]\\
&\quad+\frac{1}{2}\mu_0\left[H_0^2(V_{all} - V_1) + \frac{8\pi d^2}{3R_2^3}\right],
\end{aligned} \tag{7}$$

where V_1 is the volume of air and V_{all} is the whole space of the system. The relationship between η_s and H can be approximated as[27]

$$\eta(H) = \eta_0 + \frac{3}{2}\Phi_{hyd}\eta_0\frac{\xi - \tanh(\xi)}{\xi + \tanh(\xi)}, \tag{8}$$

where $\xi = \mu_0 mH/kT_f$ represents the ratio of magnetic energy to heat energy of a single magnetic nanoparticle, k is the Boltzmann constant, m is the magnetization denoted by $m = M_s\pi D^3/6$, T_f is the ferrofluid temperature, η is the viscosity of ferrofluid in the absence of magnetic field, $\Phi_{hyd} = \Phi_0\left(\frac{D+2\varepsilon}{D}\right)^3$ is the hydrodynamic volume fraction, ε is the thickness of magnetic particle surfactant and Φ_0 is the volume fraction of magnetic particles, and D is the diameter of the IONPs.

The Lagrangian equation is expressed as

$$\frac{\mathrm{d}}{\mathrm{d}t}\frac{\partial L}{\partial \dot{q}} - \frac{\partial L}{\partial q} = 0, \tag{9}$$

where L is defined as $L = T - U$. Substituting Eqs. (1) and (8) into Eq. (10), the dynamic equations can be written as

$$\begin{aligned}
&R_1\ddot{R}_1\left[1 + \left(\frac{\rho_L - \rho_S}{\rho_S}\right)\frac{R_1}{R_2}\right]\\
&+\dot{R}_1^2\left[\frac{3}{2} + \left(\frac{\rho_L - \rho_S}{\rho_S}\right)\left(\frac{4R_2^3 - R_1^3}{2R_2^3}\right)\frac{R_1}{R_2}\right]\\
&= \frac{1}{\rho_S}\left(\rho_L\frac{\dot{x}^2}{4} + P_{sc} - G\right),
\end{aligned} \tag{10}$$

$$\ddot{x} + \frac{3\dot{R}_2\dot{x}}{R_2} = \frac{3F_{ex}}{2\pi\rho_L R_2^3}. \tag{11}$$

Equation (11) governs oscillation and equation (12) controls translational motion. G is the correlation term affected by the magnetic field, which can be expressed as

$$\begin{aligned}
G = \frac{\mu_0}{6}\Bigg\{&\frac{4c\dot{c}(1+\chi)}{R_1^5} - \frac{6c^2(1+\chi)}{R_1^6}\\
&+2\left[a\dot{a} - b\dot{b}(1+\chi)\right]R_1\\
&+\frac{3\left[-2d^2 + 2c^2(1+\chi) + a^2R_2^6\right]}{R_1^6}\\
&+\frac{4d\dot{d} - 4c\dot{c}(1+\chi) + 2b\dot{b}(1+\chi)R_2^6 - 3H_0^2R_2^3R_1^2}{R_2^3R_1^2}\Bigg\},
\end{aligned} \tag{12}$$

where $\dot{a}$, $\dot{b}$, $\dot{c}$, and $\dot{d}$ are the first order derivatives with a, b, c, and d, respectively.

Obviously, both magnetic and ultrasound fields affect the behavior of MMBs. Numerical methods play an important role in insight into physical processes, it can provide detailed and non-destructive information on mechanical processes that are difficult to observe biomedical application experiments *in vitro* or *in vivo*. Therefore, the influence of magnetic field on the motion of MMBs and its mechanism is studied numerically.

3. Numerical analysis

Based on the model expressed by Eqs. (10) and (11), the radial vibration, translational motion and their coupling movement are analyzed under magneto-acoustic combined field. SPIOs diameter $D = 10$ nm, $M_s = 300$ kA/m, $\Phi = 10$ %, and $T_f = 300$ K. Other parameters used in numerical analysis are summarized in Table 1.

Table 1. Physical parameters used in numerical analysis.

Parameter	Symbol	Unit	Value
Density of liquid	ρ_L	kg/m^3	1000
Density of magnetofluid	ρ_S	kg/m^3	1140
Viscosity of liquid	η_L	Pa·s	10^{-3}
Viscosity of magnetofluid ($H_0 = 0$)	η_0	Pa·s	0.01
Viscosity of phospholipid layer	η_{s0}	Pa·s	4.5×10^{-9}
Constant of the phospholipid layer	K	N/m	0.3
Internal surface tension coefficient	σ_1	N/m	0.04
External surface tension coefficient	σ_2	N/m	0.005
Ratio of specific heats	γ	1	4/3
Static pressure	P_0	Pa	1.01×10^5

3.1. Basic motion

As a carrier of drug transport, MMBs urgently need to overcome fluid flow, be magnetically guided and accumulate in the target to achieve therapeutic concentration. To investigate the performance of magnetic field control and retain mo-

tion MMBs in target, bubble's initial translation velocity is assumed to be $v_{x0} = 5$ m/s. R_{20} is set as 5 μm, 10 μm, 20 μm and $n = 1.2$, respectively and drive sound field parameters are 20 kHz and $P_a = -1.2 \times 10^5$ Pa. Figures 2(a) and 2(b) show the behavior of MMBs in magnetic field of $H_0 = 400$ kA/m (solid line), and $H_0 = 0$ (dashed line) is used as control group.

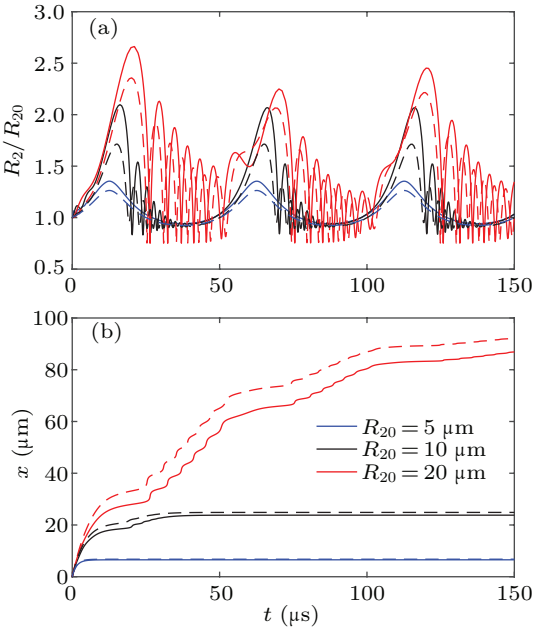


Fig. 2. Magnetic response of a moving MMB. Dashed lines are $H_0 = 0$ and solid lines are $H_0 = 400$ kA/m.

The vibration curves were shown in Fig. 2(a), the maximum expansion radius in $H_0 = 400$ kA/m is bigger than that in $H_0 = 0$, and their difference decreases with R_{20} reducing. It indicates that the magnetic field can promote the bubble expansion and the smaller bubble size, the weaker blowing effect. Besides, it is found from x–t curves in Fig. 2(b), the position coordinate x at the same time is larger in the presence of a magnetic field than $H_0 = 0$. It means the translation is blocked and the displacement is shortened by the applied magnetic field. Although the magnetic field has opposite effects on translation and oscillation, both effects decrease as the bubble size decreases. It suggests that MMBs with larger size are more sensitive to magnetic field and easier be manipulated. In addition, the strength H_0 and the initial translation speed v_{x0} are also relevant.

3.2. Regulation of v_{x0}

In Subsection 3.1, the basic motion of MMBs in $H_0 = 400$ kA/m are discussed when v_{x0} is fixed. When v_{x0} changes to 0 m/s, 3 m/s, and 5 m/s, their motion are analyzed numerically. The phase diagram of bubble and v_x–x translation curves when $R_{20} = 10$ μm and $n = 1.2$ are shown in Figs. 3(a) and 3(b) at $H_0 = 400$ kA/m, and Figs. 3(c) and 3(d) are at $H_0 = 0$ kA/m.

In Fig. 3(a), three trajectories do not change significantly when v_{x0} increases from 0 m/s to 3 m/s and then to 5 m/s, and the morphology remains as a distorted elliptical closed trajectory. It indicated that v_{x0} has almost no effect on oscillation in $H_0 = 400$ kA/m. Compared with Fig. 3(c), the range of phase diagrams in $H_0 = 0$ kA/m is smaller but their phase trajectories still coincide in different v_{x0}. The result implies that the magnetic field can be used to blow MMBs and enhance their expansion, the degree may be related to v_{x0}.

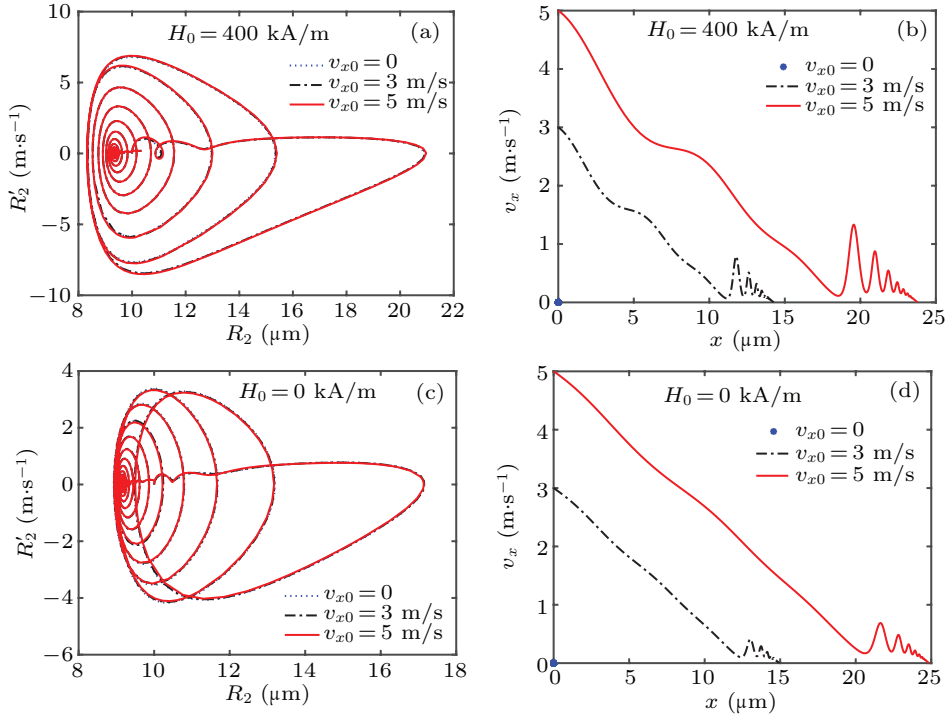


Fig. 3. MMBs response to translational initial velocity v_{x0}. $R_{20} = 10$ μm, $n = 1.2$.

In Fig. 3(b), v_x decreases nonlinearly in $H_0 = 400$ kA/m and v_x–x curves are almost parallel when $v_{x0} = 3$ m/s and $v_{x0} = 5$ m/s, the v_x decreasing trend is hardly affected by v_{x0}. External magnetic field shortened translational displacement and enhanced the fluctuation of v_x–x curves by compared with $H_0 = 0$ kA/m in Fig. 3(d). This result can be interpreted as: MMBs translation is mainly affected by liquid viscous resistance related to v_x. The magnetic field enhances the wall vibration speed, intensifies the surrounding liquid flow and increases viscous resistance, and finally leads to the reduction of translational displacement. However, it should be noted that when $v_{x0} = 0$, the bubble translational motion does not change with external magnetic field, which means that magnetic field has no effect on static bubbles.

3.3. Blowing mechanics of magnetic field

To explore the mechanism of bubble motion under magnetic field control, the additional forces due to the magnetic field were analyzed and compared with the common encapsulated MBs in absence of magnetic field. The additional forces mainly include magnetic pressure G and viscous drag force $F_{\eta s}$.[28] For a bubble with $R_{20} = 10$ μm and $n = 1.02$ at $P_a = 1.2 \times 10^5$ Pa, the curves of G–t and $F_{\eta s}$–t were show in Figs. 4(a) and 4(b) when $H_0 = 100$ kA/m, 400 kA/m, and 500 kA/m. G and $F_{\eta s}$ increase with H_0, but the two forces have different effects on bubble motion due to their opposite directions. In Fig. 4(a), G is always negative and it can enhance the vibration from Eq. (11). Compared with the curve of $F_{\eta s}$–t in Fig. 4(b), the $F_{\eta s}$ may be either positive or negative and may promote or hinder the oscillation. In this way, G and $F_{\eta s}$ compete and restrict each other during bubble vibration. Additionally, G is much larger than $F_{\eta s}$ in a strong magnetic field, which leads to vibration enhancement. This is also illustrated in Fig. 2(a), the amplitude in $H_0 = 400$ kA/m is higher than in $H_0 = 0$ kA/mm.

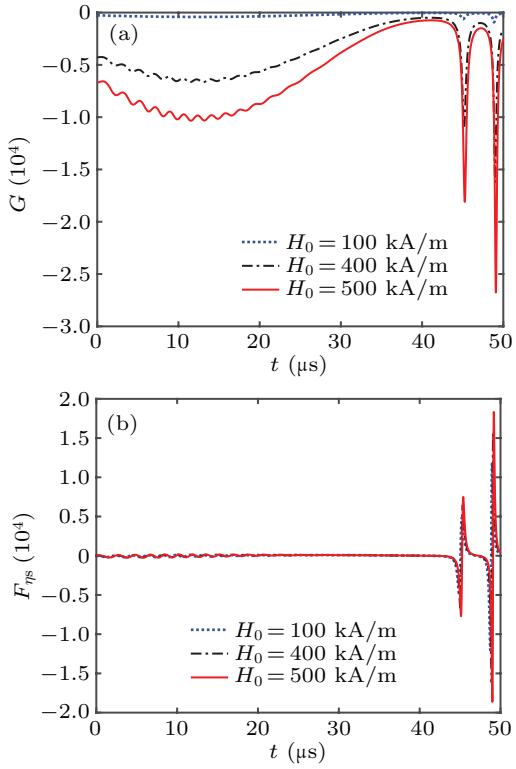


Fig. 4. Time evolution of additional forces in magnetic field: $R_{20} = 10$ μm, $n = 1.02$.

3.4. The influence of shell thickness

The expansion of the MMBs can be enhanced by magnetic field, the magnetic sensitivity is an important property and it is related to the membrane thickness n and the volume fraction of SPIOs Φ. If $\Phi = 0.1$, the thickness response to applied magnetic field is discussed. The blue stars in Fig. 5 are the maximum of R_2/R_{20} at $H_0 = 450$ kA/m when n is 1.02, 1.05, 1.08, 1.15, and 1.2. As a comparison, the red dots are used as a common UCA at $H_0 = 0$ and the maximum of R_2/R_{20} reduces as n increases, because the surface tension increases with the larger thickness. Conversely, the maximum enlarges with n in the strong magnetic field $H_0 = 450$ kA/m. This response of thickness is easy to understand. The more magnetic particles the thicker n contains, the stronger response to the applied magnetic field.

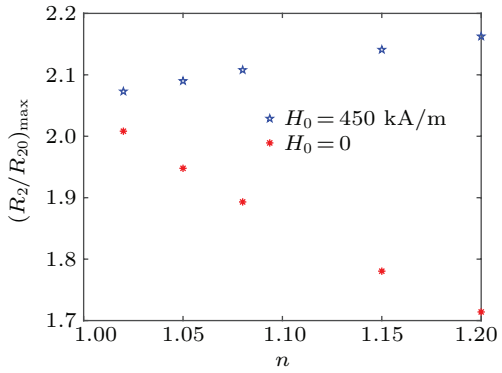


Fig. 5. Oscillation responses to the ferrofluid shell thickness: $R_{20} = 10$ μm, $P_a = 1.2 \times 10^5$ Pa.

3.5. Coupling of oscillation and translation

The red lines of x–t curves in Fig. 2(b) are step-like shape. Compared with Fig. 2(a), the step period is the same as the vibration. Does this imply a possible coupling between oscillations and translations? Zhang[29] has showed that the pulsation sound affects the resultant force in x-axis direction and eventually causes the bubble to translate. Combined Eqs. (10) and (11), it is obvious that both oscillation and translation are related to the horizontal viscous drag F_{ex}. Figure 6 gives the relationships of F_{ex}–t (blue lines) to x–t (red lines) at $H_0 = 400$ kA/m and $H_0 = 0$ for $R_{20} = 20$ μm. F_{ex} undergoes several mutations during the first acoustic period, the rapid contraction causes it to reach a minimum and v_x is maximized. With bubbles rapid translation, it begins to expand, causing F_{ex} to increase and the translation speed to slow down

and enter the next cycle. Moreover, the time of bubble's rebound is very short which makes F_{ex} change periodically, and then the translational displacement has the character of step-like change. Compared with $H_0 = 0$ (dashed line), the magnetic field increases the amplitude of F_{ex}, indicating that the reduction of translational displacement in Figs. 3(b) and 3(d) is because of the increase of magnetic field.

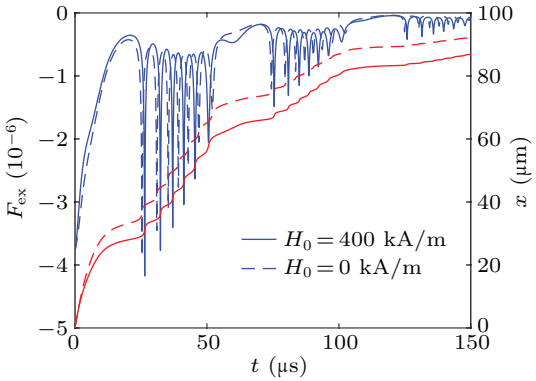


Fig. 6. The F_{ex}–t and x–t in different magnetic fields.

3.6. Comparison with the model of non-magnetic bubble in ferrofluid

Bubble dynamics in magnetic field was often treated as a non-magnetic bubble in a ferrofluid. Inspired by this idea, Chen *et al.*[23] transformed MMBs into non-magnetic bubbles in ferrofluid and established a mathematical dynamic model by Lagrange method. Although it is an indirect way to understand MMBs' response to the magnetic field, it can still be applied for experimental purposes. If our model is comparable to Chen's model, the latter can be used as an alternative experimental protocol for MMBs.

The acoustic frequency and magnetic field intensity responses are numerically analyzed. Ferrofluid is the same in two models and $\Phi = 0.1$, radius of encapsulated microbubble R_{20} are 1 μm, 5 μm, 10 μm, respectively, and shell thickness $n = 1.2$ with the driving sound pressure $P_a = 1.2 \times 10^5$ Pa. If all bubbles are non-magnetic, their resonant frequencies f are 5 MHz, 817 kHz, and 392 kHz, respectively.[21] Sweep around f and the maximum expansion rate $(R_2/R_{20})_{max}$ at $H_0 = 400$ kA/m are shown in Figs. 7(a)–7(c) and the cases of $H_0 = 0$ kA/m serves as controls (dotted-lines). The frequency response of three sizes of bubbles in two models are similar, the difference is only the location and value of the peaks. $(R_2/R_{20})_{max}$ in Chen's model decreases faster than present model, but they are close and less affected by the magnetic field when the driving frequency above their resonant frequencies. Compared $R_{20} = 1$ μm (Fig. 7(a)) to $R_{20} = 5$ μm and $R_{20} = 10$ μm in Figs. 7(b) and 7(c), vibration stability of larger bubbles in low frequency is worse than smaller one.

The responses to the magnetic field of bubble with $R_{20} = 10$ μm in two models are also investigated in Fig. 8. Figure 8(a) is the bifurcation diagram of the pulsation versus magnetic field intensity from Chen's model. The pulsation is period-one and period-double, and the curve is bifurcated at $H_0 = 785$ kA/m and closed at $H_0 = 905$ kA/m. For comparison, present model in this work as shown in Fig. 8(b), only period-one pulsation occurs and the expansion radius decreases in low intensity, which is consistent with the experiment.[30] However, our model does not exhibit pulsation disorder in a strong magnetic field, which is different from his model. Anyway, the two models are comparable in the low intensity magnetic field.

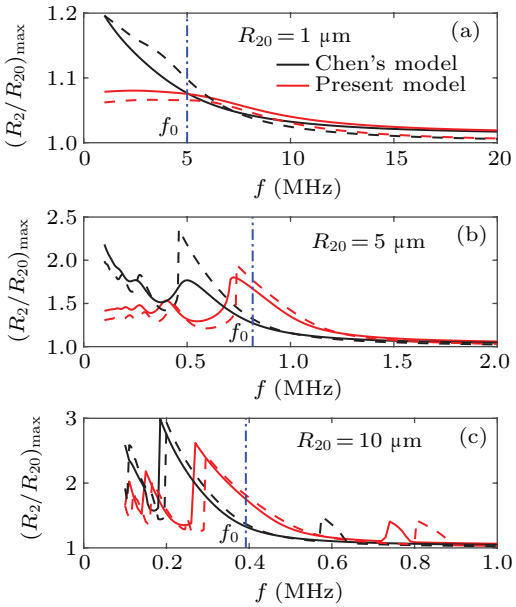


Fig. 7. Frequency responses in two models. Dashed lines are $H_0 = 0$ kA/m and solid lines are $H_0 = 400$ kA/m.

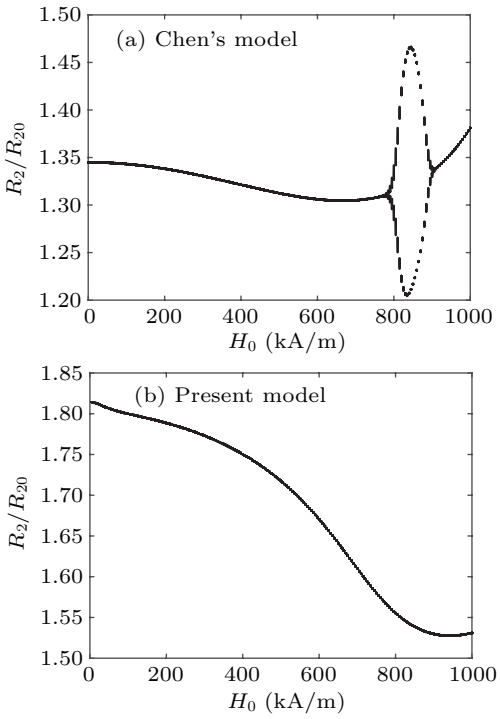


Fig. 8. Magnetic field intensity responses in two models. $R_{20} = 10$ μm.

4. Conclusion

Dynamic equations describing oscillation and translation of MMBs in magnetic-acoustic field are derived by Lagrange method and the behaviors are analyzed numerically. The magnetic field expands the bubble and shortens its translation distance, those effects diminishing as the bubble size. The initial translational velocity has almost no effect on its motion. Magnetic pressure and layer viscous force are both competitive for oscillation in the magnetic field. The magnetic pressure is stronger in a higher intensity magnetic field and makes bubble expand. The maximum expansion radius is larger than that of the ordinary encapsulated UCA and increases with the membrane thickness. In addition, the change of Levich viscous drag caused by rebound makes bubble translate in a step-like manner. Furthermore, compared with Chen's model of non-magnetic microbubbles in ferrofluid, two models are almost consistent at high driving frequency, and the relationship between the driving frequency and the resonant frequency can be judged as an alternative basis. This study is an exploration of magnetic field guiding and controlling the movement and behavior of MMBs, and may provide some suggestions for the experimental scheme for MMBs research.

Acknowledgement

Project supported by the National Natural Science Foundation of China (Grant Nos. 12074238, 11974232, and 11774212).

References

[1] Sciallero C, Balbi L Paradossi G and Trucco A 2016 *R. Soc. Open Sci.* **3** 160063
[2] Owen J, Pankhurst Q and Stride E 2012 *Int. J. Hyperth.* **28** 362
[3] Beguin E, Bau L, Shrivastava S and Stride E 2019 *ACS Appl. Mater. Interfaces* **11** 1829
[4] Zhao X, Quinto-Su P A and Ohl C D 2009 *Phys. Rev. Lett.* **102** 024501
[5] Vlaskou D, Plank C and Mykhaylyk O 2013 *Methods Mol. Biol.* **948** 205
[6] Wang S Y, Guo X X, Ren L L, Wang B, Hou L X, Zhou H, Gao Q C, Gao Y and Wang L H 2020 *Ultrason. Sonochem.* **67** 105188
[7] Qian B, Zhao Q and Ye X F 2020 *J. Cardiovasc. Pharmacol.* **76** 414
[8] Duan L, Yang F, He W, Song L N, Qiu F, Xu N, Xu L, Zhang Y, Hua Z C and Gu N 2016 *Adv. Funct. Mater.* **26** 8313
[9] Liu Y Y, Lai X S, Zhu Y, Guo F J, Su L L, Arkin G, He T Z, Xu J F and Ran H T 2022 *Int. J. Pharm.* **616** 121299
[10] Yan L P, Miao W and Li D D 2020 *J. Nanosci. Nanotech.* **20** 6087
[11] Liu Z, Lammers T, Ehling J, Fokong S, Bornemann J, Kiessling F and Gätjens J 2011 *Biomaterials* **32** 6155
[12] Marie D S V, Barnsley L C, Carugo D, Owen J, Coussios C C and Stride E 2019 *Ultrasound Med. Biol.* **45** 1151
[13] Wang S Y, Guo X X, Xiu W J, Liu Y, Ren L L, Xiao H X, Yang F, Gao Y, Xu C J and Wang L H 2020 *Sci. Adv.* **6** 8204
[14] Wang L C, Wang J N, Hao J N, Dong Z L, Wu J R, Shen G F, Ying T, Feng L Z, Cai X J, Liu Z and Zheng Y Y 2021 *Adv. Mater.* **33** 2105351
[15] Zhang B H, Wu H Y, Goel L, Kim H, Peng C, Kim J, Dayton P A, Gao Y and Jiang X N 2021 *Ultrasonics* **116** 106487
[16] Yang F, Li Y X, Chen Z P, Zhang Y, Wu J R and Gu N 2009 *Biomaterials* **30** 3882
[17] Owen J, Pankhurst Q A and Stride E 2012 *Int. J. Hyperthermia* **28** 362
[18] Stride E, Porter C, Prieto A G and Pankhurst Q 2009 *Ultrasound Med. Biol.* **35** 861
[19] Church C C 1995 *J. Acoust. Soc. Am.* **97** 1510
[20] Doinikov A A and Dayton P A. 2006 *J. Acoust. Soc. Am.* **120** 661
[21] Doinikov A A and Dayton P A. 2007 *J. Acoust. Soc. Am.* **121** 3331
[22] Lind S J. 2014 *Phys. Fluids* **26** 061901
[23] Chen J, Zhao L X, Wang C H and Mo R Y 2021 *J. Magn. Magn. Mater* **538** 168293
[24] Zhao L X, Shi H M, Bello I, Hu J, Wang C H and Mo R Y 2022 *Chin. Phys. B* **31** 034302
[25] Mulvana H, Eckersley R J, Tang M X, Pankhurst Q and Stride E 2012 *Ultrasound Med. Biol.* **38** 864
[26] Zhu G P, Nguyen N T, Ramanujan R V and Huang X Y 2011 *Langmuir* **27** 14834
[27] Malvar S, Gontijo R G and Cunha F R 2018 *J. Eng. Math.* **108** 143
[28] Doinikov A A 2002 *Phys. Fluids* **14** 1420
[29] Zhang L L, Chen W Z, Zhang Y Y, Wu Y R, Wang X and Zhao G Y 2020 *Chin. Phys. B* **29** 034303
[30] Ken H, Hiroshi N, Keiko S, Shigeo M and Yoshio T 2022 *Micron* **160** 103306